CQDs hole transport layer enhanced photocatalytic performance of $BiVO_4$-based type II heterojunctions for water splitting

Bin Wang, Guangxin He, Yan Wang, Nieyou Lin, Zihan Chen, Jie Li, Zhengbo Jiao*

Institute of Materials for Energy and Environment, College of Materials Science and Engineering, Qingdao University, Qingdao 266071, P.R. China

Characterization

Scanning electron microscope (SEM) measurements were conducted on a field emission scanning electron microscope (JSM-7800F, JEOL, Tokyo, Japan) with an acceleration voltage of 5 kW and a resolution of 0.8 nm. Transmission electron microscope (TEM) images were analyzed using the JEOL JEM-2100 Plus transmission electron microscope (Tokyo, Japan) at an accelerating voltage of 200 kV. The X-ray diffraction (XRD) patterns were obtained on a Rigaku Ultima IV instrument (Tokyo, Japan) utilizing Cu Ka radiation (40 kW) at a scanning rate of 10 degrees/min. X-ray photoelectron spectroscopy (XPS) measurements were conducted on a PHI5000 VersaProbe III (ULVAC-PHI, Japan). The vacuum was in the range of 10-9-10-10 mbar, and the X-ray source was an aluminum target with a photon energy of 1486.6 eV. The samples were prepared as homogeneous thin films or sheets that were mounted on the XPS stage. The analyzer type was a hemispherical energy analyzer, and the photoelectron pass energy for the survey spectrum was 280 eV and 69 eV for the narrow spectrum. Moreover, a dualbeam neutralization gun was utilized for automatic neutralization of the surface charge, and fitting was performed using the Gaussian Lorentzian approach. The analysis of the ultraviolet-visible (UV-vis) absorption spectra was conducted on an ultraviolet-visible spectrophotometer (UV- 2700, Tokyo, Japan). Additionally, a dual-beam system with a wavelength scanning range of 200-800 nm was used. The steady-state photoluminescence (PL) spectra were obtained

using an FLS1000 (Edinburgh, UK) at an excitation wavelength of 386 nm and a wavelength scanning range of 510‑550 nm. PEC tests were performed with a standard three-electrode system on an electrochemical workstation (CHI 660E).

Photoelectrochemical measurements

Photoelectrochemical testing was conducted at room temperature using a 0.1 M Na_2SO_4 solution as the electrolyte. A three-electrode system was employed for PEC testing: a pre-fabricated BVO-based heterojunction photoanode as the working electrode, a Pt sheet electrode as the counter electrode, and a saturated calomel electrode (SCE) as the reference electrode. Linear sweep voltammetry (LSV), transient photocurrent response (I-T), electrochemical impedance spectroscopy (EIS), and stability tests were performed on samples under AM 1.5 simulated sunlight conditions using a CHI 660E electrochemical workstation.

Calculate the bandgap width of the photoanode using the following formula:

$$(\alpha hv)^n = A\,(hv - E_g)$$

Where α is the absorption coefficient, h is Planck's constant, v is the incident light frequency, A is the proportionality constant, and Eg and n are the bandgap width and characteristic constant, respectively.

ABPE was calculated using the following formula:

$$ABPE = \frac{J(1.23 - V_{RHE})}{P_{light}} \times 100\%$$

Here, J denotes the current density obtained under applied bias, and P_{light} represents the incident light power density.

The IPCE of all photoanodes was determined by measuring the photocurrent density under specific wavelength sunlight at a voltage of 1.23 V vs RHE and calculated using the following formula:

$$IPCE = \frac{1240 \times J}{\lambda \times P_{light}} \times 100\%$$

Here, λ denotes the incident light wavelength, P_{light} represents the monochromatic light power density at each wavelength, and J indicates the photocurrent density.

The calculation formula for charge injection efficiency is as follows:

$$\eta_{inj} = \frac{J_{H_2O}}{J_{Na2SO3}} \times 100\%$$

The photocurrent densities J_{H_2O} and $J_{Na_2SO_3}$ correspond to solutions not containing and containing the Na_2SO_3 hole trap agent, respectively.

The charge separation efficiency is calculated using the following formula:

$$\eta_{sep} = \frac{J_{Na2SO3}}{Jabs} \times 100\%$$

$J_{Na_2SO_3}$ denotes the photocurrent density measured with sodium bisulfite as the electrolyte, while J_{abs} represents the theoretical maximum photocurrent density of the photoanode.

The transient photocurrent response and stability of the photoanode were tested under an applied bias voltage, and the transient decay time τr was calculated from the transient photocurrent response.

$$D = \frac{I_t - I_{st}}{I_{in} - I_{st}}$$

Here, I_t (mA/cm²) denotes the photocurrent varying with time, while I_{st} (mA/cm²) and I_{in} (mA/cm²) represent the steady-state photocurrent and initial photocurrent, respectively. The electron lifetime (τ_r) is defined as the time at which lnD = -1.

$$N_d = \frac{2}{e\varepsilon\varepsilon_0 A^2 m}$$

The formula for calculating the carrier density Nd is shown above, where e is the elementary charge (1.602×10^{-19} C), ε0 is the vacuum permittivity (8.854×10^{-14} F·cm^{-1}), ε is the relative permittivity of the semiconductor material, A is the effective illumination area of the electrode, and m is the slope of the linear region of the Mott–Schottky plot.

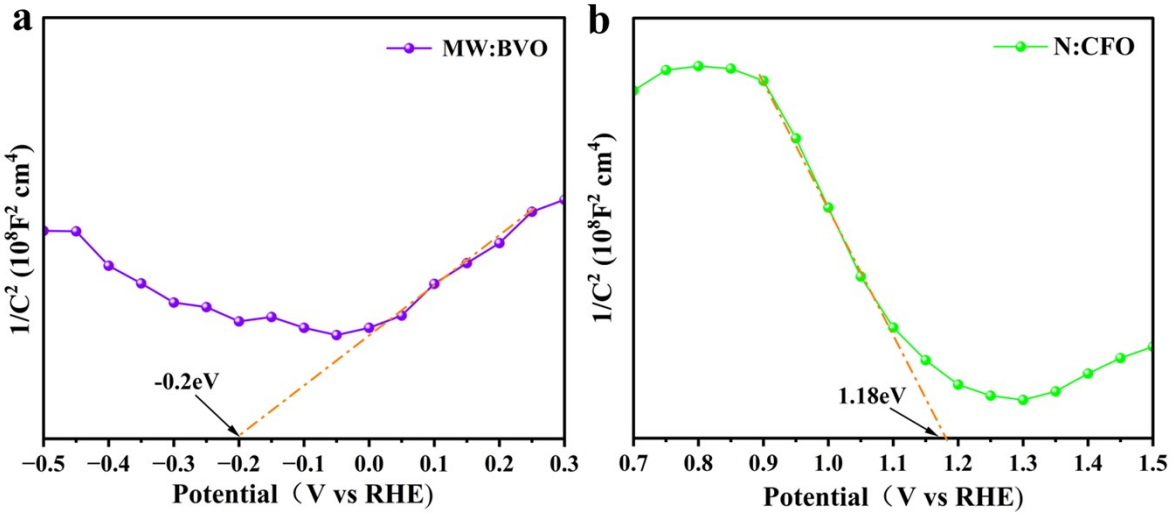

Fig. S1 Mott-Schottky plots of MW:BVO and N:CFO

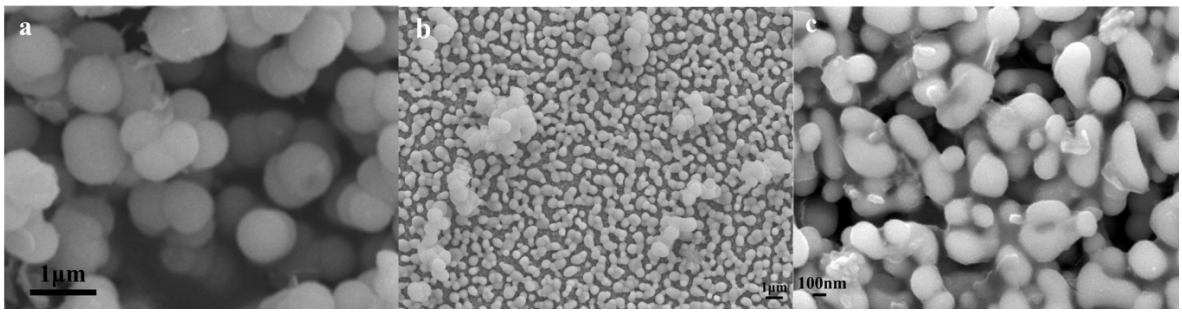

Fig. S2 SEM image of (a)N:CFO,(b) MW:BVO/N:CFO,(c) MW:BVO/CQDs

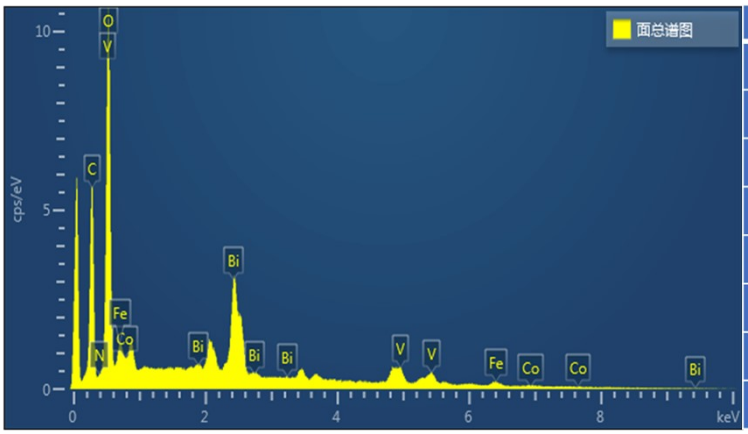

元素	wt%	原子百分比
C	20.99	40.46
N	0.11	0.16
O	34.35	49.71
V	5.13	2.33
Fe	7.14	2.96
Co	2.83	1.11
Bi	29.45	3.26
总量:	100.00	100.00

Fig.S3 Elemental content images of MW:BVO//N:CFO/CQDs

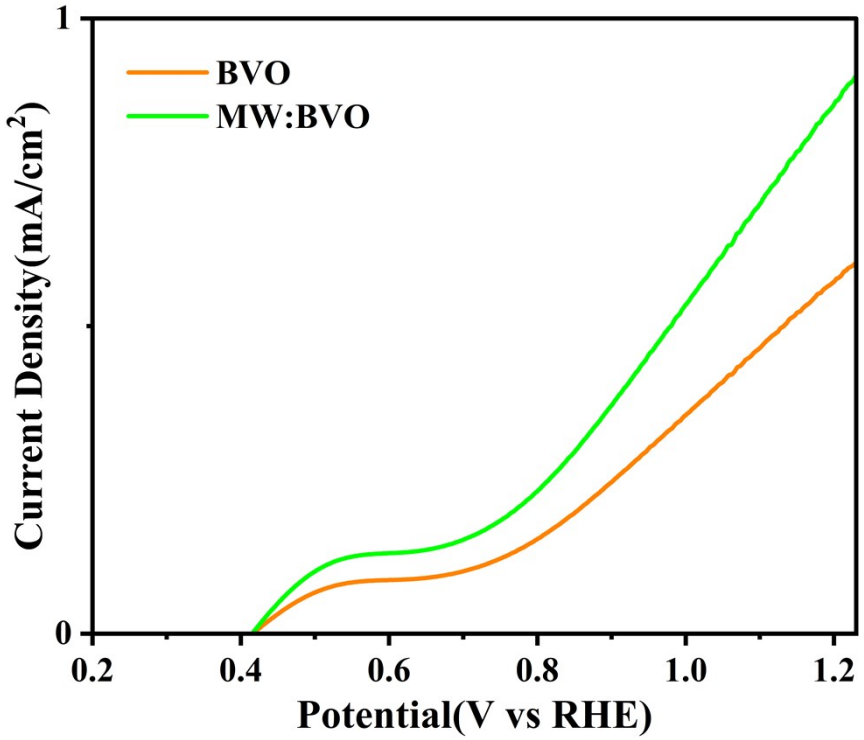

Fig. S4 LSV curve of BVO and Mo and W doped BVO.

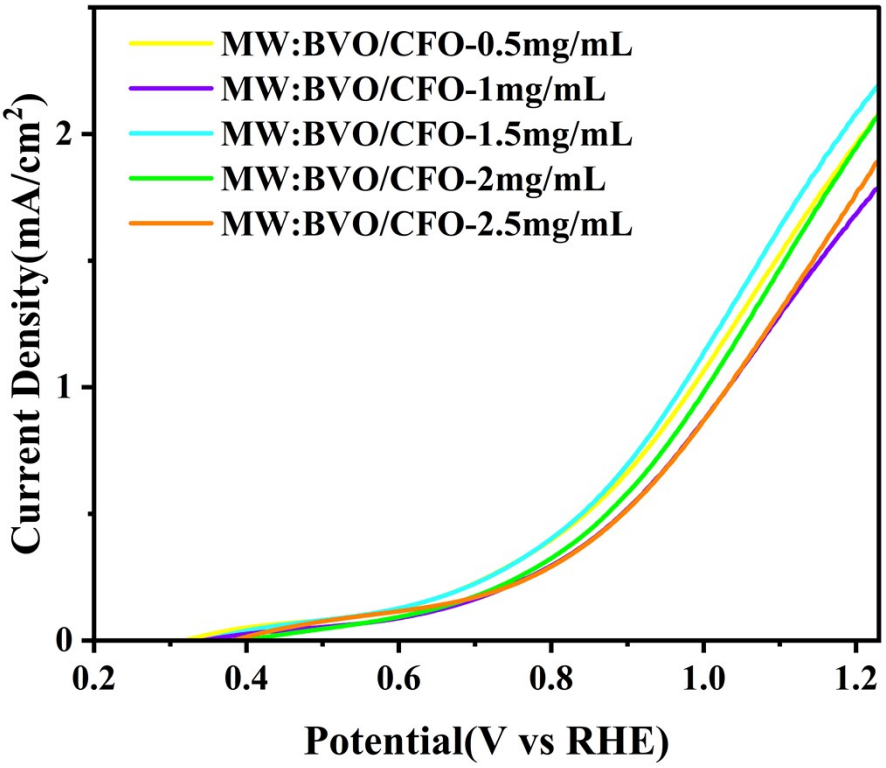

Fig.S5 LSV curves of MW:BVO/CFO with different concentrations

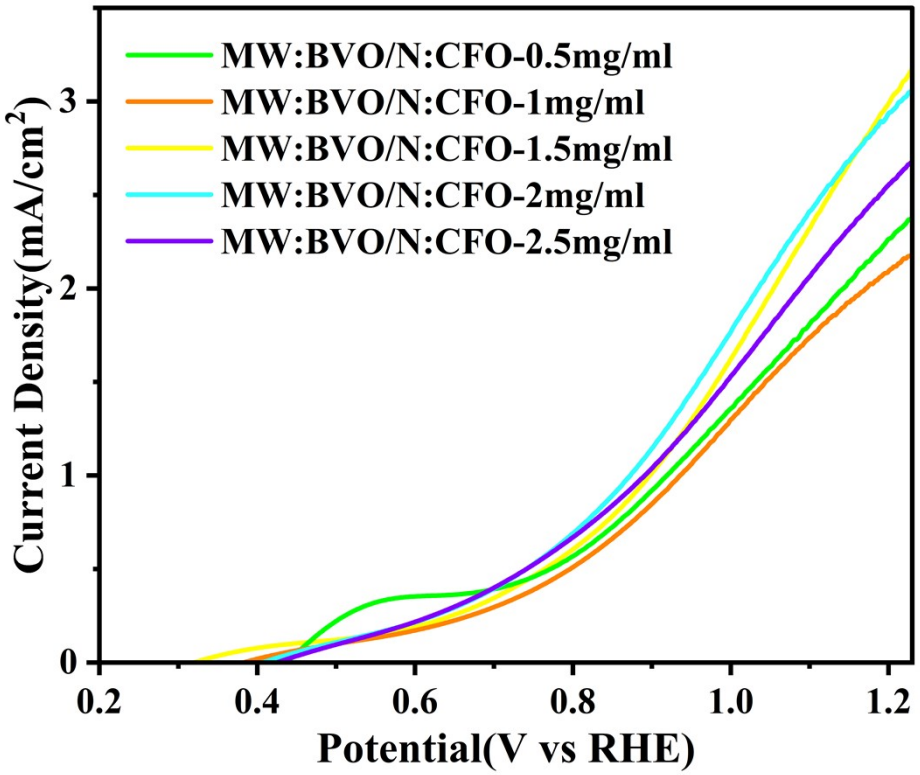

Fig. S6 LSV of MW:BVO/N:CFO with different concentrations

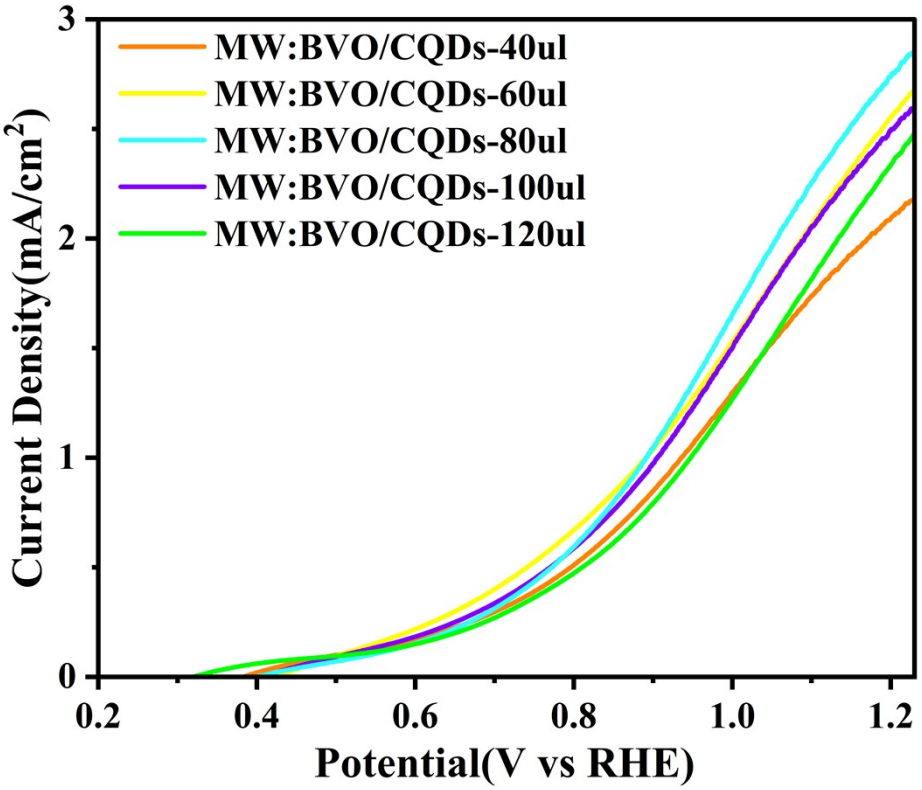

Fig. S7 LSV of MW:BVO/CQDs with different volumes

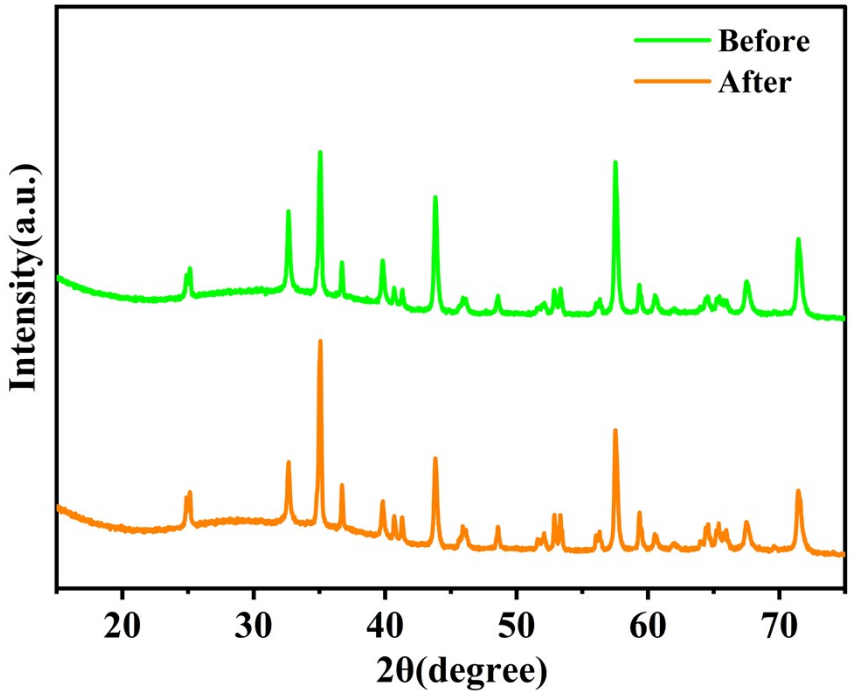

Fig. S8 XRD patterns of MW:BVO/N:CFO/CQDs

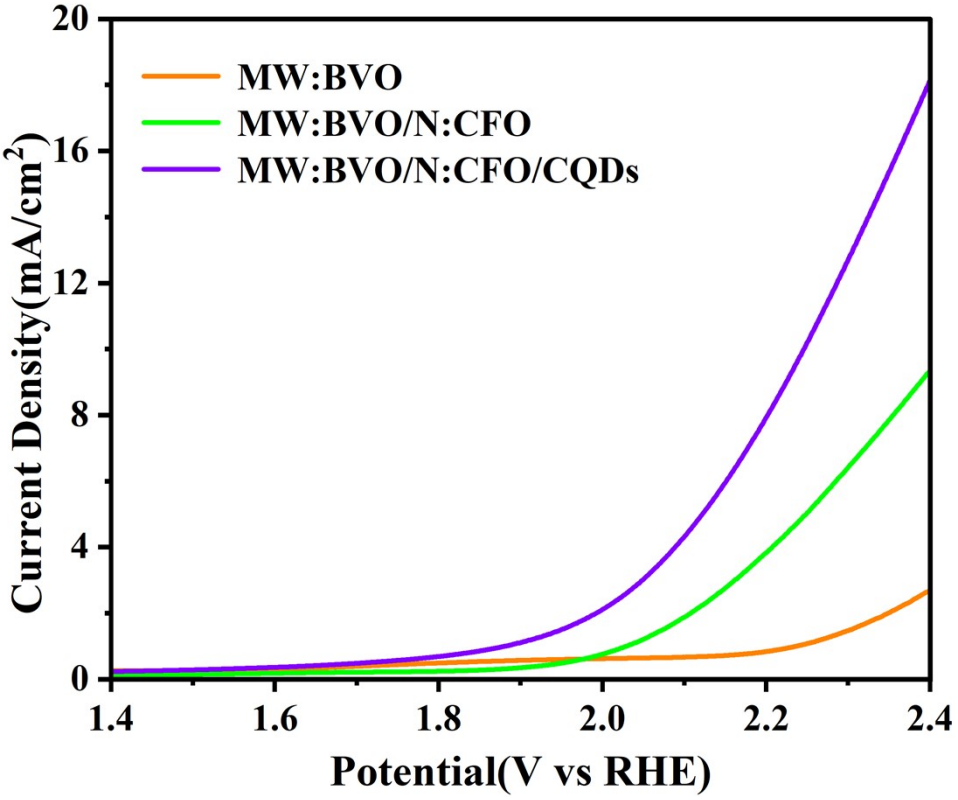

Fig. S9 LSV in the dark of MW:BVO-based photoelectrodes.

Table S1 Comparison of our photoanode to other BiVO4-based photoanodes

photoanodes	The photocurrent density at 1.23 V vs RHE (mA/cm²)	Reference
BVO/Cu_2O/Co-Pi	2.22	[1]
BVO/In_2O_3/FeOOH/NiOOH	4.0	[2]
BVO/Bi/NiMOF/CoOOH	4.7	[3]
BVO/CQDs/FeOOH	2.5	[4]
BVO/Ni_3POM/FeOOH	5.2	[5]

Table S2 EIS fitting data of MW:BVO-based photoanodes

photoanodes	R_S (Ω)	R_{CT} (Ω)
MW:BVO	23.25	19437
MW:BVO/N:CFO	23.56	13144
MW:BVO/ N:CFO/CQDs	19.25	6728

Table S3 Carrier density (Nd) of $BiVO_4$-based photoanode

Sample	Slope ($10^8 F^{-2} cm^4/V$)	Nd ($10^{21} cm^{-3}$)
MW:BVO	6.0	7.84
MW:BVO//N:CFO	4.94	9.53
MW:BVO//N:CFO/CQDs	3.88	12.13

1. X. Li, J. Wan, Y. Ma, Y. Wang and X. Li, Chemical Engineering Journal, 2020, https://doi.org/10.1016/j.cej.2020.127054.
2. D. Yin, X. Ning, Q. Zhang, P. Du and X. Lu, Journal of Colloid and Interface Science, 2023, https://doi.org/10.1016/j.jcis.2023.04.173.
3. J. Cui, M. Daboczi, M. Regue, Y. C. Chin, K. Pagano, J. Zhang, M. A. Isaacs, G. Kerherve, A. Mornto, J. West, S. Gimenez, J. S. Kim and S. Eslava, Advanced Functional Materials, 2022, https://doi.org/10.1002/adfm.202270250.
4. T. Zhou, S. Chen, J. Wang, Y. Zhang, J. Li, J. Bai and B. Zhou, Chemical Engineering Journal, 2020, https://doi.org/10.1016/j.cej.2020.126350.
5. C. Hu, C. Xu, X. Li, B. Li, X. Ma, J. Zhu, C. Dong and Y. Ding, ACS Sustainable Chemistry & Engineering, 2023, https://doi.org/10.1021/acssuschemeng.3c00114.